

## Deforming biological membranes: How the cytoskeleton affects a polymerizing fiber

D. R. Daniels<sup>a)</sup>

*Department of Physics, University of Warwick, Coventry CV4 7AL, United Kingdom*

J. C. Wang and R. W. Briehl

*Department of Physiology and Biophysics, Albert Einstein College of Medicine, Bronx, New York 10461*

M. S. Turner

*Department of Physics, University of Warwick, Coventry CV4 7AL, United Kingdom*

(Received 17 August 2005; accepted 7 November 2005; published online 10 January 2006)

We give a theoretical treatment of the force exerted by a fluctuating membrane on a polymer rod tip, taking into account the effects of an underlying biological cytoskeleton by way of a simple harmonic dependence on displacement. We also consider theoretically and experimentally the dynamics of a growing fiber tip under the influence of such a fluctuation-induced membrane force, including the effects of an underlying cytoskeletal network. We compare our model with new experimental data for the growth of hemoglobin fibers within red blood cells, revealing a good agreement. We are also able to estimate the force and membrane/cytoskeletal displacement required to stall growth of, or buckle, a growing fiber. We discuss the significance of our results in a biological context, including how the properties of the membrane and cytoskeleton relate to the thermodynamics of rod polymerization. © 2006 American Institute of Physics. [DOI: [10.1063/1.2148960](https://doi.org/10.1063/1.2148960)]

### I. INTRODUCTION AND MOTIVATION

The interactions between semiflexible intracellular rods or fibers and biological membranes<sup>1–4</sup> are of wide biological relevance, particularly where the membrane is in the presence of an underlying cytoskeletal network.<sup>5–13</sup> The filaments of interest may include, e.g., actin filaments, microtubules, or sickle hemoglobin fibers. It is therefore important to be able to obtain some measure of the influence of the cytoskeleton on the forces at work near cell membranes.<sup>14–21</sup> In this paper we consider the effects of the cytoskeleton on the force exerted by a membrane on a growing fiber. Several experimental studies have now shown how fibers can grow towards, and deform, membranes.<sup>2,5,21–25</sup> Studying the influence of the cytoskeleton on this fluctuating membrane force is relevant and important for the late-time dynamics of fiber growth,<sup>18–26</sup> as found in “biological thermal ratchets,”<sup>14–17</sup> as well as the overall stability<sup>21</sup> and possible buckling transitions<sup>22–24</sup> of rod/membrane/cytoskeleton systems, as found in cell enclosed fibers.<sup>2,3,5</sup>

In this work we will consider the compressive axial force experienced by a polymer rod in the presence of composite membranes, i.e., a fluid membrane attached to a cytoskeletal network. Such structures are found in a wide variety of cells, including in the red blood cell (RBC or erythrocyte) with its spectrin cytoskeleton.<sup>5,27</sup> The effect of the cytoskeleton on the fluctuation spectrum of such composite membranes has been experimentally observed in, e.g.,

Ref. 27. The effect of the cytoskeleton on cell membrane elasticity has been experimentally probed in, e.g., Ref. 13, via micropipette aspiration techniques.

The cytoskeleton (as in a RBC, for example) consists of a roughly two-dimensional, flexible, triangular network of proteins that is connected to a fluid membrane at many attachment points distributed over the surface.<sup>28</sup> The material of the cytoskeletal fibers itself is usually much stiffer than the fluid membrane.<sup>5,28</sup> Recently the effects of the cytoskeleton on the fluid membrane have been successfully modeled via a coarse-grained approach using continuum elasticity (see Refs. 29–31 for more details). There it is found that the effect of the attachment of the cytoskeleton is to induce an effective surface tension, along with a harmonic confining potential, on the fluid membrane. Both effects are related to the stiffness of the underlying filaments that make up the cytoskeletal network.<sup>30</sup> In order to accurately describe the mechanical properties, elasticity, fluctuation spectrum, and forces produced by the whole cell, it is important to understand the coupling between the cytoskeleton network and the associated fluid membrane.<sup>28–31</sup> Portions of the fluid membrane that are attached to the underlying cytoskeleton are much more confined with respect to fluctuations in the normal and transverse directions.<sup>30,31</sup>

Via careful consideration of both the statistical mechanics and fiber dynamics, we are able to account for the interaction between a fluctuating membrane and a fiber tip, in the presence of an underlying cytoskeletal network.<sup>29–31</sup> Most previous work<sup>14–24</sup> on this topic does not take into account the effects of the cytoskeleton. By extending our previous work<sup>32</sup> to include the effects of the cytoskeleton,<sup>29</sup> we are able to quantitatively calculate the influence of the cytoskeleton on the force generated by a fluctuating membrane on a

<sup>a)</sup>Author to whom correspondence should be addressed. Electronic mail: [d.r.daniels@warwick.ac.uk](mailto:d.r.daniels@warwick.ac.uk)

fiber tip via a “microscopic” model,<sup>30</sup> and derive the force generated as a function of the rod to membrane distance. Throughout we will assume that the membrane is impenetrable by the rod and the only interactions will be steric and therefore of very short range.

By considering membrane fluctuations in the presence of a cytoskeleton, we are also able to parametrize the influence of the cytoskeleton on the strength of the membrane-induced force on a growing rod tip in terms of the underlying membrane/cytoskeleton composite elastic constants.<sup>30</sup> Our theory for fiber growth dynamics in the presence of a cytoskeleton is then able to accurately model experimental data, obtained from growing hemoglobin fibers inside red blood cells, as described below. The consequences of our model for the thermodynamics and kinetics of rod/membrane/cytoskeleton systems will be discussed later in this article.

## II. THEORY

We parametrize our membrane and its fluctuations via the variable  $u(x, y)$ , which measures the deviation of our membrane from local flatness,<sup>1,4</sup> which we take to be the  $x$ – $y$  plane ( $u=0$ ). We assume throughout that the lateral size of the membrane is sufficiently large so that all physical results are relatively insensitive to the shape of the membrane boundary.

For the purposes of this work, we will use the following harmonic free energy (see the Appendix for discussion of when this formalism remains valid) for the displacement  $u(x, y)$ :<sup>1,4,29,30</sup>

$$F_u = \frac{1}{2} \int d^2x (\kappa (\nabla_{\perp}^2 u)^2 + \sigma (\nabla_{\perp} u)^2 + \gamma u^2), \quad (1)$$

which contains an “effective” surface-tension ( $\sigma$ ) term, a rigidity ( $\kappa$ ) term, and a cytoskeleton confinement ( $\gamma$ ) term.<sup>29,30</sup> Note that the free energy (1) is only strictly valid for relatively small displacements of  $u$  (see the Appendix for further details).

The effects of the cytoskeleton on the membrane are twofold.<sup>29</sup> Firstly, the last term in Eq. (1) governs the effect of the cytoskeleton on the fluid membrane via an effective harmonic, confining, potential of strength  $\gamma$ . This represents an approximate treatment of the effect of the cytoskeleton. Such a harmonic potential term is typically absent for membranes without a cytoskeleton.<sup>1,4</sup> Secondly, the cytoskeleton contributes to the second term in Eq. (1) via a renormalization of the “bare” surface tension  $\sigma_0$ <sup>30,31</sup> as follows. In the absence of a cytoskeleton, the membrane may possess an intrinsic surface tension of  $\sigma_0$ . Due to the presence of a cytoskeleton, this intrinsic (or bare) surface tension becomes “renormalized” to  $\sigma = \sigma_0 + (\sigma - \sigma_0)$  where the contribution of the cytoskeleton to the measured surface tension of the membrane/cytoskeleton composite is given by  $(\sigma - \sigma_0)$ . Note that in this coarse-grained picture the numerous discrete attachment points of the membrane to the cytoskeleton are not explicitly included in the continuum elastic model.<sup>30</sup> Rather, in this approach, it is precisely the effect of these contact points that ultimately give rise to the effective, confining, harmonic potential, and renormalized surface tension for the

fluid membrane due to the underlying cytoskeletal network.<sup>30</sup> For a microscopic justification and motivation for using the phenomenological Eq. (1) see Refs. 29–31 for further details, where the parameters  $\gamma$  and  $\sigma$  are shown to be related to the microscopic structure of the cytoskeleton and the underlying properties of the cytoskeleton/membrane coupling.

We now proceed to consider the form of the coupling between our membrane and the tip of a polymer rod lying along the  $\hat{\mathbf{k}}$  axis. Note that we assume the rod tip to be “pointlike,” which is a valid approximation as long as the rod radius is less than the “mesh size” of the membrane (which is typically found to be the case experimentally). To begin with, we fix the midpoint fluctuations of our membrane, directly above the tip, to be some fixed but arbitrary value,  $z$ , and calculate the partition function as follows (unless otherwise stated we adopt energy units in which  $k_B T = 1$  throughout):

$$Z_z = \int Du \delta(u(0,0) - z) \exp(-F_u). \quad (2)$$

Using the Fourier decomposition:  $u(x) = \int [d^2p / (2\pi)^2] u(p) e^{ip \cdot x}$ , we can straightforwardly carry out the functional integral<sup>33</sup> in Eq. (2), so as to arrive at the following expression for  $Z_z$ :

$$Z_z = \exp(-Cz^2), \quad (3)$$

where we have defined for convenience the constant  $C$ , which depends on the characteristic parameters of our membrane/cytoskeleton composite as

$$C = \frac{2\pi\sqrt{\sigma^2 - 4\kappa\gamma}}{\ln[(\sigma + \sqrt{\sigma^2 - 4\kappa\gamma})/(\sigma - \sqrt{\sigma^2 - 4\kappa\gamma})]}. \quad (4)$$

Note that  $Z_z$  in Eq. (3) represents the partition function for the midpoint fluctuations of our membrane, fixed at some arbitrary value  $z$ . Note also in Eq. (4) that all the elastic constants ( $\kappa, \sigma, \gamma$ ) effectively combine to produce a single elastic constant  $C$  that governs the strength of the midpoint fluctuations of our membrane. One can easily convince oneself [from inspection of Eq. (4)] that an increase in  $\sigma$  and  $\gamma$  (due to the influence of the cytoskeleton) always produces a concomitant increase in the single, effective, elastic constant  $C$ . When the cytoskeleton is absent, it can also be shown<sup>32</sup> that  $C$  approaches  $C \rightarrow \frac{2\pi\sigma_0}{\ln(\sigma_0\Omega/\kappa\pi^2)}$ , where  $\Omega$  is the area of the membrane.

In order to complete the calculation of the partition function for our cytoskeleton/membrane composite, including the presence of the rod, we need to further integrate  $Z_z$  from the position of the tip of the rod,  $\Delta$ , to  $\infty$ . This procedure realizes the physical constraint that we wish to impose, namely, that the membrane midpoint must fluctuate entirely above the rod tip and never below it. So we write (introducing a convenient normalization)

$$Z_{\Delta} = \frac{\int_{\Delta}^{\infty} dz Z_z}{\int_{-\infty}^{\infty} dz Z_z} = \frac{1}{2} (1 - \operatorname{erf}(\sqrt{C}\Delta)), \quad (5)$$

where  $\Delta$  is the position of the tip along the  $\hat{\mathbf{k}}$  axis.

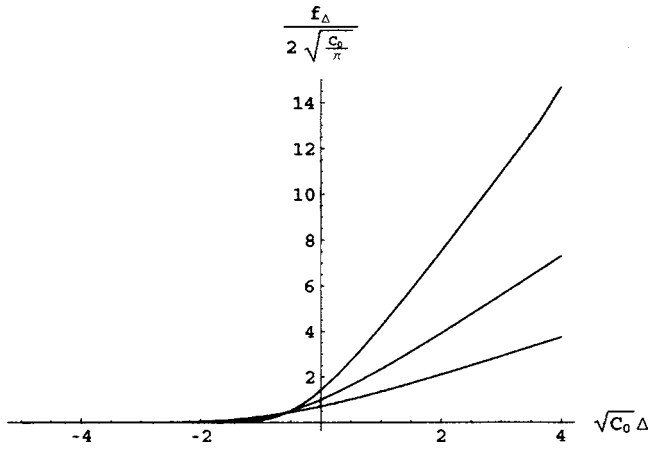


FIG. 1. Plot of the scaled force exerted by the membrane,  $f_{\Delta}/2\sqrt{C_0/\pi}$ , against the scaled distance of the tip from the membrane,  $\sqrt{C_0}\Delta$ . From top to bottom  $C/C_0=2, 1$ , and  $0.5$ , with  $C_0$  held fixed.

### A. Effect of the cytoskeleton on typical membrane forces generated

From Eq. (5) we are now in a position to simply calculate the force exerted by the membrane, in the presence of an underlying cytoskeleton, on the polymer rod tip as follows:<sup>32</sup>

$$f_{\Delta} = -\frac{\partial \ln(Z_{\Delta})}{\partial \Delta} = 2\sqrt{\frac{C}{\pi}} \frac{\exp(-C\Delta^2)}{1 - \operatorname{erf}(\sqrt{C}\Delta)}. \quad (6)$$

In order to get a representative measure of the influence of the cytoskeleton on the force generated by our membrane/cytoskeleton composite on a rod, we have plotted in Fig. 1 the force, as given by Eq. (6), against membrane to tip distance, for three values of the elastic constant  $C$ . From Fig. 1 we can see that the effect of the underlying cytoskeleton, via an increase in the elastic constant  $C$  (corresponding to an increase in  $\sigma$  and  $\gamma$ ) is to give rise to a resulting increase in the force experienced by our rod. Furthermore, from Fig. 1 we can discern the following behavior of our rod/membrane/cytoskeleton system. For large, positive  $\Delta$ , the rod tip strongly distorts the membrane upwards, and the force generated by the cytoskeleton/membrane on the tip,  $f_{\Delta} \rightarrow 2C\Delta$ , then becomes Hookean with a spring constant given by  $\approx 2C$ . So we can clearly see, in this limit, that an increase in  $C$ , due to the effect of the cytoskeleton, produces an increase in the force. As  $\Delta \rightarrow 0$ , when the tip reaches the average position of the unperturbed (flat) membrane, the force is  $2\sqrt{C/\pi}$ , which again increases as the effect of the underlying cytoskeleton increases. Lastly, when the rod tip is very far away from the membrane ( $\Delta$  large and negative), the force generated by the cytoskeleton/membrane decays away rapidly to zero (as one would expect), whether there is a cytoskeleton present or not. Therefore one conclusion to be drawn from the above is that the presence of the cytoskeleton produces a greater resulting force per unit membrane extension, than when the cytoskeleton is absent. For a comparison of typical force magnitudes predicted by our model versus those typically found experimentally, see Appendix.

### III. ROD GROWTH DYNAMICS IN THE PRESENCE OF A CYTOSKELETON

We are now in a position to investigate the effect of the cytoskeleton on the growth dynamics of a polymerizing rod, as can be found experimentally, for example, within the context of hemoglobin fibers within RBCs.<sup>2,5</sup> The dynamics of a growing fiber (as found in “Brownian ratchet” models)<sup>14–17</sup> is conditioned by the rate of monomer addition,  $\alpha = k_{\text{on}}[M]\delta$ , and the rate of monomer removal,  $\beta = k_{\text{off}}\delta$ , where  $\delta$  is a monomer size. It is typically assumed that the rate of monomer addition to the fiber depends on the concentration of locally available monomers at the tip,  $[M]$ , whereas the rate of monomer removal does not. Note, that in what follows we assume that available monomers are able to diffuse easily to the locally growing fiber tip (see, e.g., Ref. 14 for an example of when this may not be the case). This assumption is tantamount to asserting that, in this work, we take the rate-limiting step for fiber growth to be controlled by the time for the cytoskeleton/membrane to fluctuate so as to admit a monomer to the growing tip, and not the diffusion constant of the monomers.<sup>14,26</sup>

We now proceed to give an approximate, “mean-field” type or “quasi-equilibrium,”<sup>32</sup> description for rod growth dynamics in close proximity to a fluctuating membrane, taking into account the effects of an underlying cytoskeleton. Such an approach is valid in our case since typical membrane fluctuations are much faster than typical rates of fiber growth. Indeed, for most cases of biological interest and under normal physiological conditions, such a separation of time scales is almost always observed experimentally. In the case of when the cytoskeleton is absent, already more complicated dynamical models can be found in the literature.<sup>14–20,34</sup> For the purposes of this work, however, where we do include the presence of a cytoskeleton, we prefer to use as simple and tractable a model as possible. Nevertheless, the model used in this work manages to capture the underlying effects of the cytoskeleton, and furthermore renders the underlying physics of the cytoskeleton as transparent as possible. Moreover, in the “reaction-limited” case as studied here, it can be shown (see, for example, Ref. 14) that Eq. (7) below can be derived from more complicated dynamical models, in the absence of a cytoskeleton. A similar approach to the one presented here was successfully used to model fiber growth dynamics in the absence of a cytoskeleton.<sup>32</sup> Thus, using the results of previous sections and Ref. 32, we can straightforwardly write down the (averaged over membrane fluctuations) dynamical equation obeyed by the fiber tip, in the presence of a cytoskeleton, as<sup>14–17</sup>

$$\frac{d\Delta}{dt} = \alpha \exp(-f_{\Delta}\delta) - \beta, \quad (7)$$

where  $\alpha$  is the rate of monomer addition,  $\beta$  is the rate of monomer removal, and  $\delta$  is a typical monomer size. The presence of a local force  $f_{\Delta}$  acting on the growing rod tip, enters Eq. (7) via elementary Kramers transition rate theory<sup>14,15</sup> with  $f_{\Delta}\delta$  the work required to move the membrane up one monomer size  $\delta$  from the growing tip. This energy depends on the total displacement  $\Delta$  of the tip. In this

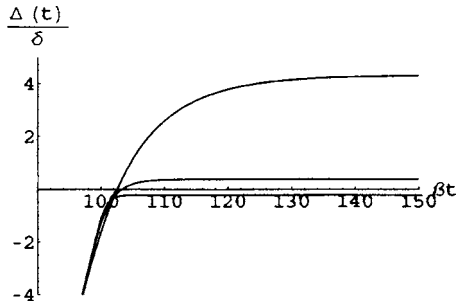


FIG. 2. Plot of (normalized) theoretically expected fiber tip position vs (normalized) time, with  $\alpha/\beta=2.0$ . From top to bottom:  $\sqrt{C\delta^2}=0.25, 0.50$ , and  $0.75$ .

work we assume typically, as in Refs. 14 and 15, for example, that only the rate of monomer addition becomes modified under the action of the local force, while the rate of monomer removal remains unaffected by  $f_{\Delta}$ .<sup>14,15</sup> Although this assumption is both reasonable and plausible for the fibers discussed here, it is conceivable that it may be relaxed for the modeling of some other biological fibers.<sup>15,18,19</sup> The current experimental record, however, remains unclear on this broad issue, so that for the purposes of this work, it seems appropriate in the first instance to use as simple a model as possible which is consistent with and able to accurately describe the experimental data (in particular, for hemoglobin as outlined below), while awaiting further experimental work that may be able to shed more light on the general validity of this assumption.

In order to clarify the physical picture of the fiber growth process, we can make the following analytic and qualitative progress, for both the early and late time regimes. When the fiber tip is far away from the membrane (i.e., small membrane force), we can approximate Eq. (7) as  $d\Delta/dt=\alpha-\beta$ , which leads to  $\Delta\propto t$  characteristic behavior at early times. Alternatively, when the fiber tip deforms the membrane strongly (i.e., large membrane force), close to the fiber growth stall threshold  $\Delta_{\text{stall}}$  calculated below, Eq. (7) reduces to  $d\Delta/dt=-2C\delta\beta(\Delta-\Delta_{\text{stall}})$ , which leads to  $\Delta\propto\exp(-2C\delta\beta t)$  characteristic behavior at late times, as the growing fiber approaches the stalled state.

More quantitatively, using Eq. (6) for  $f_{\Delta}$  we can solve Eq. (7) for  $\Delta\equiv\Delta(t)$  numerically, as shown in Fig. 2. The numerical time evolution of the position of the fiber tip shown in Fig. 2 is for three different values of  $\sqrt{C\delta^2}$  for a fixed value of the rate constants for monomer addition and removal  $\alpha/\beta$ . The parameter  $\sqrt{C\delta^2}$  measures the strength of the effect of the underlying cytoskeleton. A high value of  $\sqrt{C\delta^2}$  corresponds to a more rigid, hard-wall-type membrane, when the effects of the underlying, confining cytoskeleton are largest. A small value of  $\sqrt{C\delta^2}$  corresponds to a more flexible, highly fluctuating surface, when the effects of the underlying, confining cytoskeleton are weakest. A typical range of values of  $\sqrt{C\delta^2}\sim 0.1-1$  can be found experimentally (see the Appendix and Refs. 2, 14, 22, 29, 31, and 35). We can see from Fig. 2 that (for a given polymerization rate) the larger the confining effect of the underlying cytoskeleton on the membrane, the sooner fiber growth begins to stall. Conversely, the weaker the effect of the cytoskeleton on the

membrane, the later fiber growth stalls. From Fig. 2 we can also see that the late-time, asymptotic value of  $\Delta(t)$  is larger when the effects of the cytoskeleton are smaller. One can understand these results qualitatively in terms of the influence of the underlying cytoskeleton on membrane fluctuations. The weaker the confining effects of the cytoskeleton, the less the local, average force exerted on the fiber tip as fiber approaches the membrane. Furthermore, when the effects of the cytoskeleton are weak, the membrane is more likely on average to be able to accommodate the placement of a monomeric unit at the fiber tip, than when the effects of the cytoskeleton are strong, thus ameliorating steric constraints, and allowing the rod to grow for longer.

Additionally, it can also be shown that increasing the rate of monomer addition (polymerization rate) makes the fiber tip approach its late-time, asymptotic position more quickly, and that furthermore this late-time, fiber tip stall value increases as the rate of monomer addition increases. This can also be understood in terms of the influence of the cytoskeleton on membrane fluctuations as follows. Increasing the rate of monomer addition implies that, for the fiber tip to stall, a greater force needs to be exerted by the cytoskeleton/membrane. Now, if the cytoskeleton/membrane elastic constants are held fixed, then in order to produce the required stall force, the cytoskeleton/membrane must be deformed to a concomitantly higher degree, hence producing a greater, late-time, asymptotic value of the fiber tip position.

### A. Stalling of fiber growth and the cytoskeleton

Via inspection of Eq. (7), it is straightforward to see that rod growth stalls when the following condition holds:<sup>14,15</sup>

$$f_{\Delta\text{stall}} = \frac{1}{\delta} \ln\left(\frac{\alpha}{\beta}\right). \quad (8)$$

Equation (8) expresses the simple idea that rod growth stalls when the energy gain (or loss of entropy) produced by adding a monomer to the growing tip, exactly balances the corresponding energy cost of doing the required work against the deforming cytoskeleton/membrane. If we focus on the large  $\Delta$  Hookean regime (likely to be of most interest for stalling), we find that the onset of stalling occurs when,

$$\Delta_{\text{stall}} \approx \frac{1}{2C\delta} \ln\left(\frac{\alpha}{\beta}\right), \quad (9)$$

where  $C$  is as given by Eq. (4). From Eq. (9) we can see that  $\Delta_{\text{stall}}$  decreases as  $C$  increases (i.e., as the effect of the cytoskeleton increases).

### B. Fiber buckling and the cytoskeleton

It is also of likely interest to investigate the effect of the cytoskeleton on the buckling of polymerizing rods, as is typically found experimentally within the context of hemoglobin fibers and RBCs, for example.<sup>2,5</sup> Linear stability analysis<sup>22-24</sup> for a rod of length  $L_{\text{rod}}$ , and intrinsic stiffness  $\kappa_{\text{rod}}$ , shows that a rod will buckle (Euler buckling) when the local force applied at the rod tip reaches the critical value<sup>22-24</sup>

$$f_{\text{buckle}} = \kappa_{\text{rod}} \frac{\pi^2}{L_{\text{rod}}^2}. \quad (10)$$

Equating the critical force,  $f_{\text{buckle}}$  of Eq. (10), with the force exerted by the cytoskeleton/membrane composite, given by  $f_{\Delta}$  of Eq. (6), we can solve for  $\Delta_{\text{buckle}}$ . In particular, if we focus on the large  $\Delta$  Hookean regime (likely to be of most interest for buckling) we find that the onset of buckling occurs when,

$$\Delta_{\text{buckle}} \approx \frac{\kappa_{\text{rod}} \pi^2}{2CL_{\text{rod}}^2}, \quad (11)$$

where  $C$  is again given by Eq. (4). We can also see from Eq. (11) that, characteristically,  $\Delta_{\text{buckle}}$  decreases as the effect of the cytoskeleton increases (i.e., as  $C$  increases). For typical biological fibers, such as hemoglobin, actin, and microtubules, it is experimentally found that membrane forces are produced in roughly the region of 1–100 pN, corresponding to membrane displacements broadly in the range of 1–10  $\mu\text{m}$ .

### C. Bundles of fibers

Many growing fibers can form bundles consisting of a number  $n$  of parallel fibers. In keeping with the mean-field-type approach outlined in this work, we crudely incorporate the effects of fiber bundling into our model by simply rescaling the monomer size  $\delta$ , the monomer addition rate  $k_{\text{on}}$ , and the monomer removal rate  $k_{\text{off}}$  as follows:

$$\begin{aligned} \delta &\rightarrow \frac{\delta}{n}, \\ k_{\text{on}} &\rightarrow k_{\text{on}} n, \\ k_{\text{off}} &\rightarrow k_{\text{off}} n. \end{aligned} \quad (12)$$

The first relation in Eq. (12) merely reflects the fact that  $n$  growing fibers in parallel must (*on average*) advance a distance of  $\delta/n$  in order for the unit growth to be  $\delta$ . For this we must assume that on average the length of an entire bundle advances by one unit, smoothly and uniformly, as monomers are gradually added to all  $n$  filaments. The second and third relations in Eq. (12) take into account the simple fact that in a bundle of  $n$  fibers there are  $n$  times more active polymerization (and depolymerization) sites available to the growing fiber. Finally, note that under the rescaling of Eq. (12), we recover the desirable result that the measured growth rates of fiber lengthening,  $\alpha = k_{\text{on}}[M]\delta$ , and fiber shortening  $\beta = k_{\text{off}}\delta$ , remain at their experimentally observed values. We expect the above mean-field type of approach to fiber bundling to be a rather good approximation since it is physically unreasonable to expect (and more importantly not observed experimentally) that any one of the  $n$  fibers in will vastly outgrow any of the others in a bundle. Rather, on average, all  $n$  fibers will grow at nearly the same steady rate, thus leading to the scaling relations outlined above.

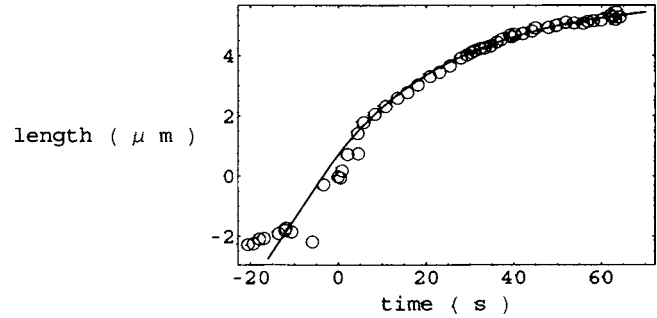


FIG. 3. Plot of experimental data vs model prediction of fiber length vs time for hemoglobin fiber 1 inside a RBC.

### IV. COMPARISON WITH EXPERIMENT

Shown in Figs. 3 and 4 are the results of fitting Eq. (7) (as described below) to experimental data<sup>36</sup> on the growth of hemoglobin fibers confined within red blood cells.<sup>37</sup> This comparison should be regarded as a limited example and is primarily intended to demonstrate the potential application of our model. The experimental procedure was as follows (see Refs. 36 and 37 for further details). A hemoglobin fiber was grown inside a red blood cell by producing deoxyhemoglobin via photolysis of CO hemoglobin. This was observed using differential interference contrast (DIC) microscopy and its length recorded. Changes in photolytic intensity altered the polymerization kinetics of the fibers, with low intensity corresponding to slow growth. The samples used were approximately 21 mM hemoglobin in 0.1M potassium phosphate (pH, 7.2). After equilibration with CO, excess CO was removed in order to minimize solution CO concentration and hence the intensity of illumination needed for photolysis. For further experimental details on the materials and methods used, the reader is again referred to Refs. 36 and 37. Returning to Figs. 3 and 4, in both plots one can see characteristically linear growth with time at early times, when the fiber is far away from the RBC cytoskeleton/membrane, followed by a gradual slowing down of growth as the fiber approaches the cytoskeleton/membrane. Note that the origins of the model prediction plots for both of the fibers have been shifted slightly so as to lie on top of the respective experimental data.

The best-fit parameters used to model the experimental data are shown in Table I. Although the number of parameters quoted in Table I may seem large, this is not really the

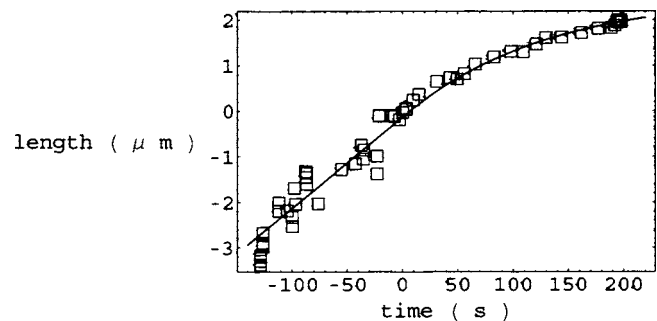


FIG. 4. Plot of experimental data vs model prediction of fiber length vs time for hemoglobin fiber 2 inside a RBC.

TABLE I. Model parameters used to fit the experimental data on hemoglobin fiber growth inside a RBC.

	$\alpha(\mu\text{m s}^{-1})$	$\beta(\mu\text{m s}^{-1})$	$\kappa \times 10^{-20}(\text{J})$	$\sigma \times 10^{-6}(\text{J m}^{-2})$	$\gamma \times 10^6(\text{J m}^{-4})$	$n$	$\delta_0(\text{nm})$
Fiber 1	0.99	0.77	2.0	1.2	1.5	10	0.45
Fiber 2	0.79	0.77	2.0	1.2	1.1	39	0.45

case, as most are already strongly delimited by preexisting and independent experimental measurements. For example, the experimentally measured values of  $\beta$  (or  $k_{\text{off}}$ ) and  $\delta_0$  for hemoglobin fibers are well known from previous work,<sup>38–40</sup> and are in excellent agreement with the model fit parameters used in this work. Therefore, given  $\beta$  and  $\delta_0$ , the model parameter  $\alpha$  (or  $k_{\text{on}}$ ) is more or less fixed by the experimentally observed early time, linear growth behavior of a hemoglobin fiber (independent of the effects of the membrane/cytoskeleton). Furthermore, the experimentally measured value of  $\kappa$  for RBCs is also well documented,<sup>13,27–29,41</sup> and is in excellent agreement with the fit parameter used here. The parameters  $\sigma$  and  $\gamma$  for RBCs have also been studied recently<sup>29,31</sup> via an analysis of the fluctuation spectrum data of Ref. 27, and are found to be comparable with the model fit parameters shown in Table I. Additionally, it is typically found experimentally<sup>39,40,42</sup> that hemoglobin fibers tend to form bundles consisting of a number  $n$  of parallel fibers. While a precise and independent experimental determination of the number of fibers in a bundle is extremely difficult, the values of  $n$  used in this work are at least reasonable, and moreover consistent with the available experimental data.<sup>39,40,42</sup> Lastly, we should mention that for the purposes of fitting we have rescaled the monomer size parameter  $\delta$  in our model for both fibers, via the consistency relation  $\delta = \delta_0/n$ , in order to take into account fiber bundling, as explained above.

## V. DISCUSSION AND CONCLUSIONS

The experimental data presented in this work on hemoglobin and RBCs, as well as other recent experiments,<sup>23,24</sup> lead us to consider a single fiber in close proximity to a fluctuating membrane, in the presence of a cytoskeleton. The fiber can grow or shrink by the accretion of monomeric units (typically for our case from one end only—we do not describe “treadmilling” here). Examples of such fibers are actin filaments, microtubules, or as in our case hemoglobin fibers.<sup>41</sup> We consider a single fiber confined within a vesicle or a red blood cell.<sup>2,5</sup> Under certain conditions such fibers have a tendency to grow in length, and as usual this is due to a free-energy imbalance between monomers in solution and those contained in the fiber. As the end of a growing fiber starts to approach the cell membrane and cytoskeleton, it is subject to a longitudinal compressive confining force. We outlined a theory for the force exerted by a fluctuating biological membrane on a polymer rod tip, including the effects of an underlying cytoskeleton. We explicitly and quantitatively derive the perturbative membrane force acting on a fiber tip via a “microscopic” model, and were furthermore able to parametrize the strength of this induced force in terms

of the membrane and cytoskeleton underlying “elastic constants.” There is a greater resulting force per unit membrane extension when the cytoskeleton is present.

We also studied the influence of the cytoskeleton on the dynamics of a growing fiber tip under the action of an induced membrane force. The model outlined in this work for fiber growth dynamics in the presence of a cytoskeleton was able to accurately describe the presented experimental data obtained from growing hemoglobin fibers inside red blood cells. Using the dynamical approach given in this work we were able to conclude that the presence of an underlying cytoskeletal network causes a growing fiber to stall (and/or buckle) sooner than would be the case if the cytoskeleton was absent. The results obtained in this work are likely to have a direct bearing on many related biological systems of interest, such as in cell motility,<sup>2,3,14,15,21,22</sup> polymerizing microtubules confined in cells or vesicles,<sup>15,22,25</sup> and other membrane enclosed fibers or rods,<sup>2,3</sup> such as actin. Extension of the model presented in this work to include the effects of spontaneous membrane curvature and/or membranes of spherical topology is left to future work.

It is of interest to briefly discuss here a method for the simultaneous extraction of the fiber rigidity and applied (membrane) force in the presence of a cytoskeleton, from measurements of the bending fluctuations of the fiber. It has previously been reported how measurements of the mode spectrum of fiber fluctuations can be used to determine their rigidities.<sup>42,43</sup> A similar technique can be employed for confined fibers, in the presence of a cytoskeleton as considered in this work (see Ref. 32 for further details). This gives a new mechanism for mapping the thermodynamics of fiber assembly under the influence of a membrane/cytoskeleton system.

Finally, the work presented here can be viewed as an alternative and “ultralocal” method for probing the properties of biological cytoskeletal networks, that is in addition and complimentary to other well-established methods such as analysis of the fluctuation spectrum of cells,<sup>27</sup> micropipette aspiration,<sup>13</sup> as well as other micromanipulation techniques. Indeed, such future experimental work may provide a further and more refined test of the theory outlined in this work.

## ACKNOWLEDGMENT

The work was supported by NIH Grant No. HL 58512 from the National Heart Lung and Blood Institute.

## APPENDIX: MODEL BREAKDOWN DISPLACEMENT AND FORCE

Our free energy for membrane displacements, as given by Eq. (1), typically assumes<sup>1,4</sup> that the excess area produced by membrane height fluctuations (over some reference base

plane) is relatively small. This translates into the condition that our model breaks down<sup>1,4</sup> whenever  $\nabla_{\perp}u \sim 1$ , locally, anywhere over the entire membrane surface. In order to quantitatively predict when this breakdown occurs we need to find the average local membrane shape,  $\langle u(x,y) \rangle$ , as a function of the in-plane membrane coordinates  $x$  and  $y$ , in the presence of the rod tip. Minimizing our free energy, Eq. (1), subject to the boundary conditions on the membrane edges, and the midpoint, we find that the shape of the membrane is given by

$$u(x,y) = \frac{z}{g(0,0)}g(x,y), \quad (\text{A1})$$

where the Green function  $g(x,y)$  satisfies

$$(\gamma - \sigma \nabla_{\perp}^2 + \kappa \nabla_{\perp}^4)g(x,y) = \delta(x)\delta(y). \quad (\text{A2})$$

In order to calculate the average membrane shape in the presence of the tip, we need to further average over the tip position such that

$$\langle u(x,y) \rangle = \frac{\langle z \rangle}{g(0,0)}g(x,y), \quad (\text{A3})$$

where now  $\langle z \rangle$  is given by

$$\langle z \rangle = \frac{\int_{\Delta}^{\infty} dz z Z_z}{\int_{\Delta}^{\infty} dz Z_z} = \sqrt{\frac{1}{\pi C} \frac{\exp(-C\Delta^2)}{1 - \text{erf}(\sqrt{C}\Delta)}}, \quad (\text{A4})$$

and is a function of the tip height  $\Delta$ . Note that what we calculate here is the *average* displacement of the membrane, which is only nonzero due to the presence of the tip. In the absence of a tip, the average displacement of a membrane must strictly vanish. Using the rotational symmetry present, introducing  $r = \sqrt{x^2 + y^2}$  (such that the tip now sits at  $r=0$ ), and converting to Fourier modes, we find that

$$\begin{aligned} g(r) &= \int_0^{\infty} \frac{p dp}{2\pi} \frac{J_0(pr)}{\gamma + \sigma p^2 + \kappa p^4} \\ &= \frac{1}{2\pi\kappa} \frac{1}{\omega_+^2 - \omega_-^2} (-K_0(\omega_+ r) + K_0(\omega_- r)), \end{aligned} \quad (\text{A5})$$

where  $J_0(x)$  and  $K_0(x)$  are the familiar Bessel functions of zeroth order, and we have defined for convenience  $\omega_{\pm} = \sqrt{\sigma/2\kappa \pm \sqrt{\sigma^2/4\kappa^2 - \gamma/\kappa}}$ .

We are now in a position to write  $\langle \nabla_{\perp}u \rangle$  as

$$\begin{aligned} \langle \nabla_{\perp}u \rangle &= \frac{\langle z \rangle}{g(0)} \frac{\partial g(r)}{\partial r} \\ &= \frac{\langle z \rangle}{\ln(\omega_+/\omega_-)} (\omega_+ K_1(\omega_+ r) - \omega_- K_1(\omega_- r)). \end{aligned} \quad (\text{A6})$$

Maximizing Eq. (A6) with respect to  $r$  (in the  $r \rightarrow 0$  limit), it can be straightforwardly shown that  $\langle \nabla_{\perp}u \rangle$  has its maximum value,  $\langle \nabla_{\perp}u \rangle_{\text{max}}$ , when approximately,

$$\langle \nabla_{\perp}u \rangle_{\text{max}} \simeq \frac{2}{5} \langle z \rangle \frac{(\omega_+^2 - \omega_-^2)}{\ln(\omega_+/\omega_-)} \omega_+^{-\omega_+^2/(\omega_+^2 - \omega_-^2)} \omega_-^{\omega_-^2/(\omega_+^2 - \omega_-^2)}. \quad (\text{A7})$$

The condition for breakdown of our model can now be finally expressed as occurring when the average membrane

displacement reaches a maximum value,  $\langle z \rangle_{\text{max}}$ , of

$$\langle z \rangle_{\text{max}} \simeq \frac{5 \ln(\omega_+/\omega_-)}{2(\omega_+^2 - \omega_-^2)} \omega_+^{\omega_+^2/(\omega_+^2 - \omega_-^2)} \omega_-^{-\omega_-^2/(\omega_+^2 - \omega_-^2)}. \quad (\text{A8})$$

Using this result for  $\langle z \rangle_{\text{max}}$ , we can also calculate the maximum force  $f_{\text{max}}$  capable of being generated in our model before it breaks down, which is given simply by

$$f_{\text{max}} \simeq 5\pi\kappa\omega_+^{\omega_+^2/(\omega_+^2 - \omega_-^2)} \omega_-^{-\omega_-^2/(\omega_+^2 - \omega_-^2)}. \quad (\text{A9})$$

Inserting typical membrane values, as probed experimentally,<sup>29-31</sup> of  $\kappa \sim 2.0 \times 10^{-20}$  J,  $\sigma \sim 1.2 \times 10^{-6}$  J m<sup>-2</sup>, and  $\gamma \sim 1.3 \times 10^6$  J m<sup>-4</sup>, we find that  $\langle z \rangle_{\text{max}} \sim 700$  nm and  $f_{\text{max}} \sim 3$  pN, which are consistent with typically expected experimental values for membrane displacements and forces as found in Refs. 2, 22, and 24, for example. Thus the theory outlined in this work is capable of providing a reasonable quantitative account of typical experimentally measured membrane forces and displacements.<sup>2,22,35</sup> Furthermore, the analysis carried out in this Appendix, validates *a posteriori* the initial use of a harmonic free energy for membrane displacements, which consequently also validates the resulting Hookean behavior of the force at relatively large membrane displacements.

<sup>1</sup> P. M. Chaikin and T. C. Lubensky, *Principles of Condensed Matter Physics* (Cambridge University Press, Cambridge, 2000).

<sup>2</sup> D. Boal, *Mechanics of the Cell* (Cambridge University Press, Cambridge, 2001).

<sup>3</sup> L. Mahadevan and P. Matsudaira, *Science* **288**, 95 (2000).

<sup>4</sup> S. A. Safran, *Statistical Thermodynamics of Surfaces, Interfaces and Membranes* (Addison-Wesley, Reading, MA, 1994).

<sup>5</sup> B. Alberts, A. Johnson, J. Lewis, M. Raff, K. Roberts, and P. Walter, *Molecular Biology of the Cell* (Garland, New York, 2002).

<sup>6</sup> H. Strey, M. Peterson, and E. Sackmann, *Biophys. J.* **69**, 478 (1995).

<sup>7</sup> D. Discher, N. Mohandas, and E. A. Evans, *Science* **266**, 1032 (1994).

<sup>8</sup> V. Heinrich, K. Ritchie, N. Mohandas, and E. Evans, *Biophys. J.* **81**, 1452 (2001).

<sup>9</sup> H. Engelhardt, H. Gaub, and E. Sackmann, *Nature (London)* **307**, 378 (1984).

<sup>10</sup> J. C.-M. Lee and D. E. Discher, *Biophys. J.* **81**, 3178 (2001).

<sup>11</sup> F. Brochard and J. F. Lennon, *J. Phys. (Paris)* **36**, 1035 (1975).

<sup>12</sup> M. Peterson, H. Stray, and E. Sackmann, *J. Phys. II* **2**, 1273 (1992).

<sup>13</sup> E. Evans and W. Rawicz, *Phys. Rev. Lett.* **79**, 2379 (1997).

<sup>14</sup> C. S. Peskin, G. M. Odell, and G. F. Oster, *Biophys. J.* **65**, 316 (1993).

<sup>15</sup> M. Dogterom, M. E. Janson, C. Faivre-Moskalenko, A. van der Horst, J. Kerssemakers, C. Tanase, and B. M. Mulder, *Appl. Phys. A: Mater. Sci. Process.* **75**, 331 (2002).

<sup>16</sup> A. Mogilner and G. Oster, *Eur. Biophys. J.* **28**, 235 (1999).

<sup>17</sup> G. S. van Doorn, C. Tanase, B. M. Mulder, and M. Dogterom, *Eur. Biophys. J.* **29**, 2 (2000).

<sup>18</sup> M. Dogterom and B. Yurke, *Science* **278**, 856 (1997).

<sup>19</sup> A. B. Kolomeisky and M. E. Fisher, *Biophys. J.* **80**, 149 (2001).

<sup>20</sup> A. E. Carlsson, *Phys. Rev. E* **62**, 7082 (2000).

<sup>21</sup> E. Evans, V. Heinrich, L. Ludwig, and W. Rawicz, *Biophys. J.* **85**, 2342 (2003).

<sup>22</sup> D. K. Fygenson, J. F. Marko, and A. Libchaber, *Phys. Rev. Lett.* **79**, 4497 (1997).

<sup>23</sup> D. K. Fygenson, M. Elbaum, B. Shraiman, and A. Libchaber, *Phys. Rev. E* **55**, 850 (1997).

<sup>24</sup> E. Elbaum, D. K. Fygenson, and A. Libchaber, *Phys. Rev. Lett.* **76**, 4078 (1996).

<sup>25</sup> A. Desai and T. J. Mitchison, *Annu. Rev. Cell Dev. Biol.* **13**, 83 (1997).

<sup>26</sup> D. J. Odde, *Biophys. J.* **73**, 88 (1997).

<sup>27</sup> A. Zilker, H. Engelhardt, and E. Sackmann, *J. Phys. (Paris)* **48**, 2139 (1987).

<sup>28</sup> V. Bennett, *Biochim. Biophys. Acta* **988**, 107 (1989).

<sup>29</sup> N. Gov, A. G. Zilman, and S. Safran, *Phys. Rev. Lett.* **90**, 228101 (2003).

- <sup>30</sup>N. Gov and S. A. Safran, Phys. Rev. E **69**, 011101 (2004).
- <sup>31</sup>J.-B. Fournier, D. Lacoste, and E. Raphael, Phys. Rev. Lett. **92**, 018102 (2004).
- <sup>32</sup>D. R. Daniels and M. S. Turner, J. Chem. Phys. **121**, 7401 (2004).
- <sup>33</sup>H. Kleinert, *Path Integrals in Quantum Mechanics, Statistics, and Polymer Physics* (World Scientific, Singapore, 2004).
- <sup>34</sup>M. Dogterom and S. Leibler, Phys. Rev. Lett. **70**, 1347 (1988).
- <sup>35</sup>A. R. Evans, M. S. Turner, and P. Sens, Phys. Rev. E **67**, 041907 (2003).
- <sup>36</sup>J. C. Wang and R. W. Briehl (unpublished).
- <sup>37</sup>R. W. Briehl, J. Mol. Biol. **245**, 710 (1995).
- <sup>38</sup>G. Agarwal, J. C. Wang, S. Kwong, S. M. Cohen, F. A. Ferrone, R. Josephs, and R. W. Briehl, J. Mol. Biol. **322**, 395 (2002).
- <sup>39</sup>R. W. Briehl and A. E. Guzman, Blood **83**, 573 (1994).
- <sup>40</sup>F. A. Ferrone, J. Hofrichter, and W. A. Eaton, J. Mol. Biol. **183**, 591 (1985).
- <sup>41</sup>W. A. Eaton and J. Hofrichter, Adv. Protein Chem. **40**, 63 (1990).
- <sup>42</sup>J. C. Wang, M. S. Turner, G. Agarwal, S. Kwong, R. Josephs, F. A. Ferrone, and R. W. Briehl, J. Mol. Biol. **315**, 601 (2002).
- <sup>43</sup>M. S. Turner, J. C. Wang, C. Jones, F. A. Ferrone, R. W. Briehl, and R. Josephs, Langmuir **18**, 7182 (2002).